Line Impedance Estimation based on Synchrophasor Measurements for Power Distribution Systems

Paolo Attilio Pegoraro, *Member, IEEE*, Kyle Brady, *Student Member, IEEE*, Paolo Castello, *Member, IEEE*, Carlo Muscas, *Senior Member, IEEE*, Alexandra von Meier, *Member, IEEE*

***Abstract*— Effective monitoring and management applications on modern distribution networks require a sound network model and the knowledge of line parameters. Network line impedances are used, among other things, for state estimation and protection relay setting. Phasor Measurement Units (PMUs) give synchronized voltage and current phasor measurements, referred to a common time reference (coordinated universal time). All synchrophasor measurements can thus be temporally aligned and coordinated across the network. This feature, along with high accuracy and reporting rates, could make PMUs useful for the evaluation of network parameters. However, instrument transformer behavior strongly affects parameter estimation accuracy. In this paper, a new PMU-based iterative line parameter estimation algorithm for distribution networks, which includes in the estimation model systematic measurement errors, is presented. This method exploits the simultaneous measurements given by PMUs on different nodes and branches of the network. A complete analysis of uncertainty sources is also performed, allowing the evaluation of estimation uncertainty. Issues related to operating conditions, topology and measurement uncertainty are thoroughly discussed and referenced to a realistic model of a distribution network to show how a full network estimator is possible.**

***Index Terms*—electric network line parameters, phasor measurement units PMUs, power distribution lines, power system measurements, voltage and current transducers, weighted least squares.**

I. Introduction

Phasor Measurement Units (PMUs) are the latest generation of measurement devices for electric grids, designed to measure synchronized voltage and current phasors across a network, as well as their frequencies and corresponding rates of change [1]. These devices are usually installed for the monitoring of transmission networks, where they have been a remarkable improvement over older sensors thanks to the availability of absolute phase angle measurements and of time-coordinated and unprecedentedly accurate measurements of the quantities of interest. Recently, with the advent of PMUs designed for distribution systems such as μPMUs [2], synchrophasor measurements are becoming more useful at distribution level, which is the focus of this paper.

A PMU can be implemented in a standalone device or as a software functionality in an IED (Intelligent Electronic Device) [3], as well as a Virtual Object in a Cloud architecture [4]. The main characteristics of PMUs are the high reporting rate and the availability of an absolute time reference for synchrophasor evaluation. The high reporting rates, compared with the classical measurement devices in supervisory control and data acquisition (SCADA) systems, permit the evaluation of fast phenomena that can occur in the electric grid and an understanding of the dynamics of the relevant signals. The absolute time reference, usually obtained from the Global Positioning System, provides an available and reliable definition of time to every PMU in a system. This is what is used to evaluate absolute phase angle. Every measurement is timestamped, allowing for the correlation of all the measurements available in a given time instant from PMUs installed across the nodes of a network.

The data provided by PMUs are collected at Phasor Data Concentrators and forwarded to the control center to be used by the target applications [5], [6]. These data can be used in different contexts for both on-line (state estimation [7]–[9], voltage stability assessment, etc.) and off-line applications (post-mortem and statistical analysis, etc.).

PMU measurements can also be used in intelligent systems that perform network model estimation or validation. In this context, the accuracy of any measurement device is an important prerequisite for the overall accuracy of the estimation results. It is important to mention here, though, that there are many uncertainty sources that cannot be neglected [10].

It is worth recalling that, in most traditional applications, network parameter values have been assumed to be known and equal to nominal values. In many cases, network parameters have been obtained by means of theoretical calculations and off-line measurements, using geometry and conductor properties. Therefore, network parameter values used by the grid operators may be significantly incorrect [11], with differences of up to 25-30 % compared to actual values [12].

To face this problem different methods to estimate the network parameters in transmission systems have been suggested in the scientific literature. Lately, there is growing interest in the possibility of a real-time estimation based on the synchronized measurement provided by the PMUs [13]. In particular, the control center seems to be the ideal context to exploit the coordinated data given by wide area measurement

P. A. Pegoraro, P. Castello, C. Muscas are with the Department of Electrical and Electronic Engineering of the University of Cagliari, Piazza d'Armi, 09123 Cagliari, Italy (email: [paolo.pegoraro, paolo.castello, carlo]@diee.unica.it).

K. Brady, A. von Meier are with the Department of Electrical Engineering and Computer Science, University of California, Berkeley, Berkeley, California, USA (email: [kwbrady, vonmeier]@berkeley.edu).

 DOI:10.1109/TIM.2018.2861058
Publisher version:https://ieeexplore.ieee.org/abstract/document/8444098/

systems for network model estimation.

The use of synchronized phasors to estimate the network parameters in a transmission line and the effect of instrument transformers (ITs) were discussed in [14], but without a robust statistical analysis. In [15] the network parameters for short transmission lines were estimated using several methods and considering different load conditions. This made use of synchronized phasors and included noise and bias errors as measurement uncertainty. In [16] a different approach was presented, where bad measurements are identified and removed before performing the estimation, random errors for the PMU measurements are applied and the ITs are assumed to be calibrated. Recently, an alternative method for estimating the parameters of a transmission network, based on Kalman filter, was presented in [17]. The methodology takes into account the uncertainty of PMU measurements, but the transducers are considered carefully calibrated. In [18] a method of identifying the transmission network parameters was presented in which the measurement model considers the uncertainties of transducers and PMUs as referring to a Gaussian distribution.

Little attention has been paid to parameter estimation in distribution systems. As mentioned above, PMUs specifically designed for distribution systems [2] are now available and the problem has become more topical than ever. In [**?**], the feasibility of calculating the impedance of both a transformer and a line from PMU measurements for distribution networks (DNs) is investigated, but measurement device and transducer uncertainties are not included in the model. In [19] line parameter estimation is performed by means of unsynchronized measurements. Steady-state conditions are assumed and phase angle errors are neglected. In [20] an optimization-based procedure is presented to estimate the parameters from voltage and power measurements, but synchronization or measurement issues and systematic errors are not considered.

In this context, a technique relying on a PMU monitoring system and a least square approach was presented in [21], which sought to estimate line parameters together with the systematic deviations (mainly from ITs). This technique was based on a linear approximation of the measurement functions and errors and results for a small portion of a DN were reported.

In this paper, a new iterative weighted least squares (WLS) method that allows dealing with large line parameter deviations is proposed. It allows the simultaneous estimation of multiple impedances on multiple branches. Systematic errors in the measurement chain are considered in the algorithm, thus allowing them to be estimated as well.

Topological and measurement constraints are included, so that all the information available for each portion of the network can be exploited.

A full derivation of the measurement model and a meticulous uncertainty evaluation is introduced along with a strategy to speed up the algorithm based on repeated measurements and uncertainty modeling.

Equations for the evaluation of the estimation uncertainty are introduced thus allowing the definition of estimation bounds.

A detailed investigation of the influence of different constraints, changing network conditions and measurement accuracies is presented with a model of a real DN and practical issues with the measurement system are discussed.

II. Proposed Estimation Algorithm

A. Definition of the Network and Measurement Model

The proposed estimation algorithm relies on a simultaneous estimation of the network line parameters and of systematic errors, assumed to be mainly introduced by transducers as in [21]. A general measurement model can be defined from typical line models. Fig. 1 shows the single-line π-model for three connected branches that represent a small portion of a generic distribution network. Shunt capacitances at both ends of each line are neglected, as is common in distribution system modeling (see [22] for a state estimation example).

First, the notation and measurement models will be described in the context of a single branch. Then the model will be extended to present the general algorithm that operates on multiple branches and can be applied to entire networks. Considering branch (i, j) of Fig. 1, the monitoring system

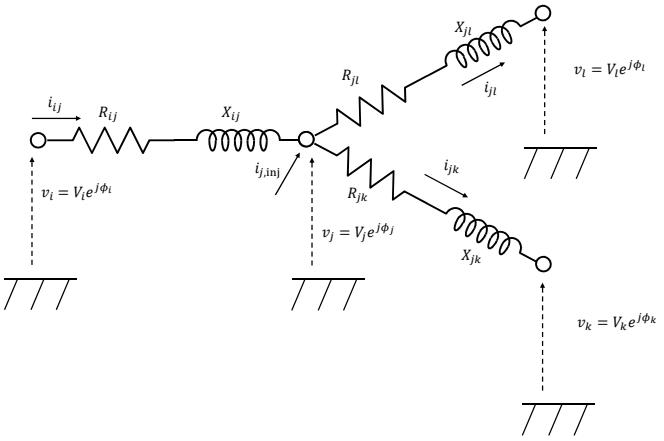

Fig. 1. Network branches model.

includes PMUs that measure the voltage synchrophasors $v_i(t)$ and $v_j(t)$ and the branch current synchrophasor $i_{ij}(t)$, where t represents the measurement time as reported in the time-tags of the data packet sent from the PMUs to the control center (at least two PMUs or two merging units communicating with suitable IEDs are needed for each branch). Measurement timestamp will be generally omitted in the following sections for the sake of brevity, and specified only when necessary.

At each time instant a set of independent measurements is collected from the field. Each phasor can be expressed as a function of its magnitude and phase angle as:

$$v_i = V_i e^{j\phi_i} \qquad v_j = V_j e^{j\phi_j} \qquad i_{ij} = I_{ij} e^{j\theta_{ij}} \tag{1}$$

The measured phasors are affected by both magnitude and phase angle errors that are introduced both by transducers and

the PMUs themselves, and can be expressed as functions of the reference quantities (indicated by a superscript 'R') as follows:

$$\begin{aligned} v_i &= (1+\xi_i+\xi_i^{random})V_i^R e^{j(\phi_i^R+\alpha_i+\alpha_i^{random})} \\ i_{ij} &= (1+\eta_{ij}+\eta_{ij}^{random})I_{ij}^R e^{j(\theta_{ij}^R+\psi_{ij}+\psi_{ij}^{random})} \end{aligned} \tag{2}$$

For both voltages and currents, the relative magnitude errors and the phase angle errors are split into two contributions of a different nature: systematic errors (represented by ξ_i and η_{ij} for magnitudes, by α_i and ψ_{ij} for phase-angles) and random errors (ξ_i^{random} and η_{ij}^{random} for magnitudes, α_i^{random} and ψ_{ij}^{random} for phase-angles). Similar quantities can be defined for all the other measured phasors (e.g. v_j).

Considering two separate contributions allows the highlighting of the different behaviors of multiple uncertainty sources. In the following, as in [21], the main source of systematic errors is associated with the transducers and thus defined by the accuracy class of the instrument transformer or divider. Random errors are mainly attributed to PMUs, and thus instrument specifications are used to quantify them. This assumption is adopted to make the presentation simple (the attribute "random" in the error notation will be replaced, in the following, by "PMU") and the tests of Section III easier to follow, but it does not exclude that random errors might result from ITs too. The model in (2) indeed allows considering both systematic and random errors without loss of generality.

Since magnitude errors introduced by transducers and PMUs are small (much lower than one), the two error contributions are presented in (2) as additive, neglecting second order terms obtained by the cascade of two ratio errors.

The relationship linking all the measurements relating to branch (i,j) (branch voltage drop equation) can be expressed as:

$$\begin{aligned} v_i^R - v_j^R &= V_i(1-\xi_i-\xi_i^{\text{PMU}})e^{j(\phi_i-\alpha_i-\alpha_i^{\text{PMU}})} \\ &\quad - V_j(1-\xi_j-\xi_j^{\text{PMU}})e^{j(\phi_j-\alpha_j-\alpha_j^{\text{PMU}})} \\ &= Z_{ij} i_{ij}^R \\ &= (R_{ij}^0(1+\gamma_{ij}) + jX_{ij}^0(1+\beta_{ij})) \\ &\quad \cdot (1-\eta_{ij}-\eta_{ij}^{\text{PMU}}) I_{ij} e^{j(\theta_{ij}-\psi_{ij}-\psi_{ij}^{\text{PMU}})} \end{aligned} \tag{3}$$

where R_{ij}^0 and X_{ij}^0 are the nominal values of (i,j)-line resistance and reactance. Parameters γ_{ij} and β_{ij} are the corresponding relative deviations from the nominal values, which will be described in the following as "correction parameters" for branch (i,j). Equation (3) is obtained under the same assumption of small ratio errors used in (2) and includes all the measurement and error quantities together with two unknowns that need to be estimated to find the impedance of the branch. This is the first complex equation of the measurement model.

From (3), further simplifications can be obtained by assuming small phase angle errors (ψ_{ij}, ψ_{ij}^{PMU}, α_i, α_i^{PMU}, α_j, and α_j^{PMU}) and applying the first-order expansion of the exponentials. This is a reasonable approximation, because ITs phase displacements are small for all the precision classes defined in the standard IEC 61869 [23], [24] and modern non-conventional transducers can have even lower errors, thus confirming the validity of the assumption. The same holds true for typical phase-angle deviations of PMUs (in the order of 10^{-3} rad for steady-state signal conditions).

Equation (3) can then be rewritten as

$$\begin{aligned} &V_i(\cos\phi_i + j\sin\phi_i)\left[1-(\xi_i+\xi_i^{\text{PMU}}) - j(\alpha_i+\alpha_i^{\text{PMU}})\right] \\ &\quad - V_j(\cos\phi_j + j\sin\phi_j)\left[1-(\xi_j+\xi_j^{\text{PMU}}) - j(\alpha_j+\alpha_j^{\text{PMU}})\right] \\ &\simeq I_{ij}(\cos\theta_{ij} + j\sin\theta_{ij})\left[R_{ij}^0(1+\gamma_{ij}) + jX_{ij}^0(1+\beta_{ij})\right] \\ &\quad \cdot \left[1-(\eta_{ij}+\eta_{ij}^{\text{PMU}}) - j(\psi_{ij}+\psi_{ij}^{\text{PMU}})\right] \end{aligned} \tag{4}$$

and, separating its real and imaginary parts, it follows:

$$\begin{aligned} &+V_i^r(1-\xi_i-\xi_i^{\text{PMU}}) + V_i^x(\alpha_i+\alpha_i^{\text{PMU}}) \\ &\quad - V_j^r(1-\xi_j-\xi_j^{\text{PMU}}) - V_j^x(\alpha_i+\alpha_i^{\text{PMU}}) \\ &\simeq I_{ij}^r R_{ij}^0(1+\gamma_{ij})(1-\eta_{ij}-\eta_{ij}^{\text{PMU}}) \\ &\quad + I_{ij}^x R_{ij}^0(1+\gamma_{ij})(\psi_{ij}+\psi_{ij}^{\text{PMU}}) \\ &\quad + I_{ij}^r X_{ij}^0(1+\beta_{ij})(\psi_{ij}+\psi_{ij}^{\text{PMU}}) \\ &\quad - I_{ij}^x X_{ij}^0(1+\beta_{ij})(1-\eta_{ij}-\eta_{ij}^{\text{PMU}}) \end{aligned} \tag{5}$$

$$\begin{aligned} &-V_i^r(\alpha_i+\alpha_i^{\text{PMU}}) + V_i^x(1-\xi_i-\xi_i^{\text{PMU}}) \\ &\quad + V_j^r(\alpha_j+\alpha_j^{\text{PMU}}) - V_j^x(1-\xi_j-\xi_j^{\text{PMU}}) \\ &\simeq I_{ij}^r X_{ij}^0(1+\beta_{ij})(1-\eta_{ij}-\eta_{ij}^{\text{PMU}}) \\ &\quad + I_{ij}^x X_{ij}^0(1+\beta_{ij})(\psi_{ij}+\psi_{ij}^{\text{PMU}}) \\ &\quad - I_{ij}^r R_{ij}^0(1+\gamma_{ij})(\psi_{ij}+\psi_{ij}^{\text{PMU}}) \\ &\quad + I_{ij}^x R_{ij}^0(1+\gamma_{ij})(1-\eta_{ij}-\eta_{ij}^{\text{PMU}}) \end{aligned} \tag{6}$$

where $V_i^r \triangleq V_i\cos\phi_i$ and $V_i^x \triangleq V_i\sin\phi_i$ are, respectively, the real and imaginary parts of the measured phasor v_i (similar definitions hold for V_j^r and V_j^x), while $I_{ij}^r \triangleq I_{ij}\cos\theta_{ij}$ and $I_{ij}^x \triangleq I_{ij}\sin\theta_{ij}$ are defined for the current. Equations (5) and (6) represent a non-linear measurement model

$$\mathbf{y}_{ij} = \mathbf{h}_{ij}(\mathbf{x}_{ij}, \mathbf{e}_{ij}), \tag{7}$$

where $\mathbf{x}_{ij} = [\xi_i, \alpha_i, \xi_j, \alpha_j, \eta_{ij}, \psi_{ij}, \gamma_{ij}, \beta_{ij}]^{\text{T}}$ is the state vector to be estimated, including all systematic errors and $\mathbf{e}_{ij} = [\xi_i^{\text{PMU}}, \alpha_i^{\text{PMU}}, \xi_j^{\text{PMU}}, \alpha_j^{\text{PMU}}, \eta_{ij}^{\text{PMU}}, \psi_{ij}^{\text{PMU}}]^{\text{T}}$ is the vector of all random contributions. $\mathbf{y}_{ij}$ represents the equivalent measurements and $\mathbf{h}_{ij}(\cdot)$ links errors to known terms (their definitions can be found in Appendix A).

The relative differences γ_{ij} and β_{ij} of the actual values of the line parameters with respect to their rated values cannot be generally considered $<< 1$ in distribution networks, where these differences can reach maximum values of few tens in percentage [25], [12], [26], [27]. Therefore the expressions in (7) (detailed in (A.1) and (A.2)) cannot be linearized. It is possible to split the second term in (7) to separate the systematic and random contributions as follows:

$$\begin{aligned} \mathbf{y}_{ij} &= \begin{bmatrix} y_{ij}^r \\ y_{ij}^x \end{bmatrix} = \begin{bmatrix} V_i^r - V_j^r - R_{ij}^0 I_{ij}^r + X_{ij}^0 I_{ij}^x \\ V_i^x - V_j^x - X_{ij}^0 I_{ij}^r - R_{ij}^0 I_{ij}^x \end{bmatrix} = \\ &= \mathbf{f}_{ij}(\mathbf{x}_{ij}) + \boldsymbol{\epsilon}_{ij}(\gamma_{ij}, \beta_{ij}, \mathbf{e}_{ij}) \end{aligned} \tag{8}$$

where $\mathbf{f}_{ij}(\cdot)$ is the measurement functions vector and $\boldsymbol{\epsilon}_{ij}$ represents the equivalent measurements random vector. Details on their elements are given in Appendix A.

Equation (8) represents the building block of the estimation, because it defines equivalent measurements for each branch and for each time instant and separates random contributions.

To estimate the branch network parameters together with the systematic errors, multiple PMU measurements of the same quantities are needed. They introduce several equations involving the same unknowns and allow for the definition of an over-determined system of equations as follows:

$$\mathbf{y}_{ij}^{tot} = \begin{bmatrix} y_{ij}^{r}(t_1) \\ y_{ij}^{x}(t_1) \\ \vdots \\ y_{ij}^{r}(t_{N_t}) \\ y_{ij}^{x}(t_{N_t}) \end{bmatrix} = \\ = \begin{bmatrix} \mathbf{f}_{ij}^{t_1}(\mathbf{x}_{ij}) \\ \vdots \\ \mathbf{f}_{ij}^{t_{N_t}}(\mathbf{x}_{ij}) \end{bmatrix} + \begin{bmatrix} \epsilon_{ij}^{t_1}(\gamma_{ij}, \beta_{ij}, \mathbf{e}_{ij}^{t_1}) \\ \vdots \\ \epsilon_{ij}^{t_{N_t}}(\gamma_{ij}, \beta_{ij}, \mathbf{e}_{ij}^{t_{N_t}}) \end{bmatrix} \quad (9)$$

where N_t is the number of timestamps under consideration.

The multiple PMU measurements corresponding to different timestamps can be classified into two types. Thanks to the high PMU reporting rates, the network evolution appears generally slow with respect to the measurement refresh timescale and thus it is possible to logically group the measurements into: measurements corresponding to different network conditions (different operation points, referred to as "cases" in the following) and repeated measurements of the same status (repeated measurements). This distinction will be adopted in the following sections to better understand the algorithm behavior.

From a practical viewpoint, this distinction can also be used to speed up the algorithm: subject to a preliminary check of the absence of rapid variations, repeating measurements in rapid succession can allow averaging to introduce equivalent measurements with higher accuracy for each case. It is possible to prove that, under the above assumptions on errors, these measurements can be used in the algorithm allowing acceleration without loss of accuracy.

The proposed estimator is designed to exploit all the available information, since the network parameter estimation process is a hard task that requires a careful definition of the uncertainty model. For this reason, it is important to use also prior information on the unknown parameters. A-priori values for the network correction parameters and for the transducer errors can be integrated into the algorithm. The former are zero since nominal values represent the best prior assumption for network parameters if no further information is given. The latter are also usually zero for similar reasons, because it is only the error ranges of the transducers that are typically known. It is thus possible to add the following constraints:

$$\mathbf{0} = \mathbf{I}_{2M_{ij}} \mathbf{x}_{ij} + \epsilon_{ij}^{prior} \quad (10)$$

where $\mathbf{0}$ is a vector of zeros, $I_{2M_{ij}}$ is the $2M_{ij} \times 2M_{ij}$ identity matrix and ϵ_{ij}^{prior} is the vector containing prior knowledge about errors. The dimension of $\mathbf{x}_{ij}$, i.e. the number of unknowns, is $2M_{ij}$: two for the impedance and two for each measurement voltage and current PMU channel relating to branch (i, j). ϵ_{ij}^{prior} is thus a vector of zero-mean random errors, the uncertainty of which can be derived from prior information on maximum deviations of the unknown parameters.

In the following, we assume that we have determined prior limits on maximum line resistance and reactance errors, as well as maximum ratio and phase displacement errors for transducers. When more accurate information is available , it can be used to redefine the uncertainties in (10) or to redefine parameters in (3).

B. Multiple Branches

The estimation algorithm is designed to estimate the impedances of multiple branches in a single process. All the synchronized measurements from across the network can be aligned and used to define a single estimation model. The following model demonstrates the consideration of a number of different branches:

$$\begin{bmatrix} \mathbf{y}_{i_1 j_1}^{tot} \\ \vdots \\ \mathbf{y}_{i_{N_{br}} j_{N_{br}}}^{tot} \end{bmatrix} = \begin{bmatrix} \mathbf{f}_{i_1 j_1}^{tot}(\mathbf{x}) \\ \vdots \\ \mathbf{f}_{i_{N_{br}} j_{N_{br}}}^{tot}(\mathbf{x}) \end{bmatrix} + \begin{bmatrix} \epsilon_{i_1 j_1}^{tot}(\gamma, \beta, \mathbf{e}) \\ \vdots \\ \epsilon_{i_{N_{br}} j_{N_{br}}}^{tot}(\gamma, \beta, \mathbf{e}) \end{bmatrix} \quad (11)$$

where $\mathbf{f}_{ij}^{tot}(\mathbf{x})$ and $\epsilon_{ij}^{tot}(\gamma, \beta, \mathbf{e})$ indicate, respectively, the vector of measurement functions and the error vectors for branch (i, j) at all instants in time. They are written as functions of the entire vector of unknowns $\mathbf{x} \triangleq \bigcup_{k=1}^{k=N_{br}} \mathbf{x}_{i_k j_k}$ (N_{br} is the number of involved branches and the union-of-sets symbol $\bigcup$ stands for a merger of all the variables of each included branch, of all the random measurement errors $\mathbf{e} \triangleq \bigcup_{k=1}^{k=N_{br}} \mathbf{e}_{i_k j_k}^{tot} = \bigcup_{k=1}^{k=N_{br}} \bigcup_{n=1}^{n=N_t} \mathbf{e}_{i_k j_k}^{t_n}$, of $\gamma = [\gamma_{i_1 j_1}, \cdots, \gamma_{i_{N_{br}} j_{N_{br}}}]^{\mathrm{T}}$ and of $\beta = [\beta_{i_1 j_1}, \cdots, \beta_{i_{N_{br}} j_{N_{br}}}]^{\mathrm{T}}$. The unknowns vector $\mathbf{x}$ includes the systematic errors of all the voltage and current measurements that are common to adjacent branches. Because the equivalent measurement errors of connected branches involve common measurements, the associated random errors are correlated as discussed in next section.

Besides the voltage drop constraints defined by (11), topological constraints are present when considering a set of branches. Two of them are particularly important for distribution networks: constraints given by injection (or, equivalently, absorption) nodes and zero injection constraints.

Looking at Fig. 1, it can be seen that the additional constraint given by the Kirchoff's current law (KCL) at a node j is:

$$i_j = \sum_{k \in \Gamma_j} i_{jk} \quad (12)$$

where Γ_j is the set of nodes adjacent to node j and $i_{jk} = -i_{kj}$ for each branch current. If the injected current phasor i_j is measured, additional equations can be added to those of (11). The details on the derivation of the constraints given by (12) are given in Appendix B (see also [21]), but the final

relationships are:

$$I_j^r - \sum_{k\in\Gamma_j} I_{jk}^r = f_j^r(\mathbf{x}) + \epsilon_j^r(\gamma,\beta,\mathbf{e}) = \eta_j I_j^r - \psi_j I_j^x + \sum_{k\in\Gamma_j}\left[-\eta_{jk} I_{jk}^r + \psi_{jk} I_{jk}^x\right] + \epsilon_j^r \tag{13}$$

$$I_j^x - \sum_{k\in\Gamma_j} I_{jk}^x = f_j^x(\mathbf{x}) + \epsilon_j^x(\gamma,\beta,\mathbf{e}) = \eta_j I_j^x + \psi_j I_j^r + \sum_{k\in\Gamma_j}\left[-\eta_{jk} I_{jk}^x - \psi_{jk} I_{jk}^r\right] + \epsilon_j^x \tag{14}$$

where η_j and ψ_j are the systematic magnitude and phase angle errors associated with the current injection measurement, similarly to other current measurements. The two random errors of the equivalent measurements defined by (13) and (14) are defined as follows:

$$\epsilon_j(\gamma,\beta,\mathbf{e}) = \begin{bmatrix} \epsilon_j^r \\ \epsilon_j^x \end{bmatrix} = \begin{bmatrix} \eta_j^{\text{PMU}} I_j^r - \psi_j^{\text{PMU}} I_j^x + \sum_{k\in\Gamma_j}\left(-\eta_{jk}^{\text{PMU}} I_{jk}^r + \psi_{jk}^{\text{PMU}} I_{jk}^x\right) \\ \eta_j^{\text{PMU}} I_j^x + \psi_j^{\text{PMU}} I_j^r + \sum_{k\in\Gamma_j}\left(-\eta_{jk}^{\text{PMU}} I_{jk}^x - \psi_{jk}^{\text{PMU}} I_{jk}^r\right) \end{bmatrix} \tag{15}$$

where the current injection PMU errors have been considered together with those of branch currents. Every node current measurement thus gives two additional constraints with two equivalent measurements that can be added to the global estimation model.

Similarly, two additional equivalent measurements are obtained when a zero-injection node is considered. The relationships in (13), (14) and (15) are simplified since no injection measurements are involved. Thus, no additional unknowns are present and the equivalent measurements link the real and imaginary current balance at a zero-injection node j to systematic errors present on the branch measurements. New couples of equivalent random errors, indicated by subscript "$j-zero$", are defined as follows:

$$\epsilon_{j-zero}(\gamma,\beta,\mathbf{e}) = \begin{bmatrix} \epsilon_{j-zero}^r \\ \epsilon_{j-zero}^x \end{bmatrix} = \begin{bmatrix} \sum_{k\in\Gamma_j}\left(-\eta_{jk}^{\text{PMU}} I_{jk}^r + \psi_{jk}^{\text{PMU}} I_{jk}^x\right) \\ \sum_{k\in\Gamma_j}\left(-\eta_{jk}^{\text{PMU}} I_{jk}^x - \psi_{jk}^{\text{PMU}} I_{jk}^r\right) \end{bmatrix} \tag{16}$$

When a full set of network branches is involved in the estimation, all the equations described above can be used to improve the performance. Prior knowledge about transducers and impedances can be inserted as was detailed in the single-branch case. Since multiple cases and repeated measurements are used, all the constraints have to be defined for each timestamp and there are then multiple equations like (15) and (16) to augment the system of (11).

C. Iterative WLS Solution

Once the whole measurement model is defined, the proposed algorithm relies on an iterative WLS estimation method, which considers, at each iteration $q+1$, the linearization of (11), (13) and (14) around the state estimated from the previous iteration q. The full system can be expressed as:

$$\mathbf{y} = \mathbf{f}(\mathbf{x}) + \epsilon \tag{17}$$

where $\mathbf{y}$ includes all the equivalent measurements (relating to branches, injections and zero injections), $\mathbf{f}(\cdot)$ is the nonlinear measurement functions vector and ϵ represents all the equivalent measurements random errors.

The aim of the iterative estimation is to achieve $\hat{\mathbf{x}} = \arg\min_{\mathbf{x}} \|\mathbf{y} - \mathbf{f}(\mathbf{x})\|_{\mathbf{\Sigma}_\epsilon}$ (where $\|\cdot\|_{\mathbf{\Sigma}_\epsilon}$ indicates the Mahalanobis norm that allows using $\mathbf{\Sigma}_\epsilon^{-1}$ as weighting matrix). Thus, at iteration q, the following solution is computed:

$$\Delta\hat{\mathbf{x}}_{q+1} = \hat{\mathbf{x}}_{q+1} - \hat{\mathbf{x}}_q = \left(\left(\left.\frac{\mathrm{d}\mathbf{f}}{\mathrm{d}\mathbf{x}^{\mathrm{T}}}\right|_{\hat{\mathbf{x}}_q}\right)^{\mathrm{T}} \mathbf{\Sigma}_{\mathbf{r}_q}^{-1} \left.\frac{\mathrm{d}\mathbf{f}}{\mathrm{d}\mathbf{x}^{\mathrm{T}}}\right|_{\hat{\mathbf{x}}_q}\right)^{-1} \cdot \left(\left.\frac{\mathrm{d}\mathbf{f}}{\mathrm{d}\mathbf{x}^{\mathrm{T}}}\right|_{\hat{\mathbf{x}}_q}\right)^{\mathrm{T}} \mathbf{\Sigma}_{\mathbf{r}_q}^{-1}\mathbf{r}_q \tag{18}$$

where $\mathbf{r}_q = \mathbf{y} - \mathbf{f}(\hat{\mathbf{x}}_q)$ is the qth iteration residual vector and $\mathbf{F}(\mathbf{x}) \triangleq \left.\frac{\mathrm{d}\mathbf{f}}{\mathrm{d}\mathbf{x}^{\mathrm{T}}}\right|_{\mathbf{x}}$ indicates the Jacobian matrix of $\mathbf{f}$ computed at the generic state $\mathbf{x}$. The iterations stop when $\|\Delta\hat{\mathbf{x}}_{q+1}\|_\infty < \delta$ (for the tests, $\delta = 10^{-7}$ will be used), that is when the state variations become negligible. The solution of (18) requires the computation of the gain matrix $\mathbf{F}(\mathbf{x})^{\mathrm{T}}\mathbf{\Sigma}_{\mathbf{r}_q}^{-1}\mathbf{F}(\mathbf{x})$ and, thus, of $\mathbf{F}(\mathbf{x}_q)$ and of the covariance matrix.

As detailed in Appendix A for branch constraints and in Appendix B for injection constraints, the Jacobian $\mathbf{F}(\mathbf{x})$ can be computed considering the partial derivatives of the functions $\mathbf{f}_{ij}$ of (8), f_j^r and f_j^x of (13), (14) and, with similar notation, of f_{j-zero}^r and f_{j-zero}^x functions, referred to all included constraints. The sub-Jacobians $\mathbf{F}_j$ and $\mathbf{F}_{j-zero}$ due to the couples of injection constraints are constant, since the corresponding functions are linear, while the sub-Jacobian $\mathbf{F}_{i,j}$ corresponding to voltage drop constraints is state dependent and, thus, iteration dependent.

Matrix $\mathbf{\Sigma}_{\mathbf{r}_q}$ can be obtained by applying the uncertainty propagation law to the equivalent measurement errors expressed as functions of the PMU errors. Excluding the equations due to prior information, the general expression is:

$$\mathbf{\Sigma}_{\mathbf{r}_q} = \mathbf{E}(\hat{\mathbf{x}}_q)\mathbf{\Sigma}_{\mathbf{e}}\mathbf{E}^{\mathrm{T}}(\hat{\mathbf{x}}_q) \tag{19}$$

where $\mathbf{E}$ is the Jacobian matrix of the error functions. In the appendices, the expressions of the errors for each type of equivalent measurement (voltage-drop, injection and zero-injection) are reported along with the corresponding submatrices of $\mathbf{E}$.

Once the complete measurement system is defined, sets of measurements relating to different timestamps are considered to be decorrelated when building the covariance matrix and prior information is treated as independent from all other equivalent measurements. When multiple branches are considered, for a single timestamp t, current injection (and zero-injection) equations introduce random errors that are correlated with the errors from the voltage drop equations for all the branches connected to the corresponding node because the

same PMU current measurements are involved. This can be seen from the submatrices of $\mathbf{E}$ in the appendices.

The vector of unknown parameters $\hat{\mathbf{x}}$ is finally estimated along with its covariance matrix:

$$\mathbf{\Sigma}_{\hat{\mathbf{x}}} = \left(\mathbf{F}(\hat{\mathbf{x}})^{\mathrm{T}} \begin{bmatrix} (\mathbf{E}(\hat{\mathbf{x}})\mathbf{\Sigma}_{\mathbf{e}}\mathbf{E}(\hat{\mathbf{x}})^{\mathrm{T}})^{-1} & \\ & \mathbf{\Sigma}_{prior} \end{bmatrix} \mathbf{F}(\hat{\mathbf{x}}) \right)^{-1} \tag{20}$$

where $\mathbf{\Sigma}_{prior}$ is the covariance matrix associated with prior information and the gain matrix of the WLS estimation is computed using the estimated values.

This algorithm can be applied to collected PMU data either online or offline. The specific implementation depends on distribution system operator needs and the available communication and computation infrastructure.

III. Tests and results

In this section, the impact of different factors on the estimation accuracy and, in particular, on the accuracy of network parameters' estimation is thoroughly investigated by means of simulations in Matlab 2017 environment. The 102-node ATLANTIDE Italian rural representative network (ATLN in the following) is used for these simulations (see Appendix C and [28]). It includes (see Fig. 2) 7 feeders with 102 medium voltage (MV) nodes supplied by one high voltage to medium voltage (HV/MV) substation. It is mostly composed of small-cross-sectional overhead lines with total length of about 160 km. The overall nominal load (a mix of agricultural, residential and small industrial customers) is about 20.21 MVA at the peak. In the following, each branch number is given by the node number of its end node decreased by one.

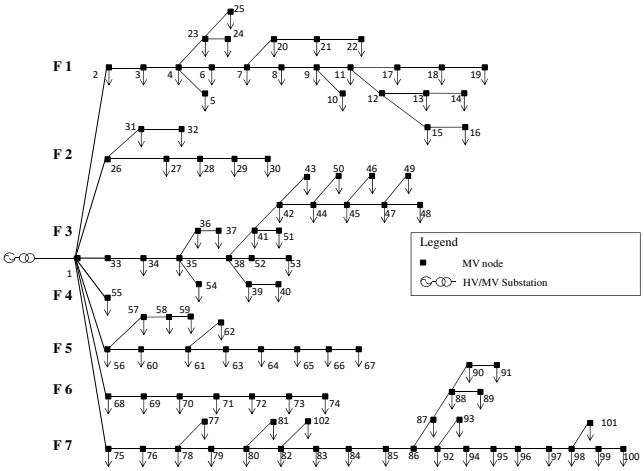

Fig. 2. ATLANTIDE project rural network.

All the tests described in this section consider a coordinated monitoring infrastructure composed of PMUs (for instance μPMUs) located at each node and measuring all the node voltage and branch current synchrophasors. While this would be prohibitively expensive at present PMU prices, as costs decrease we expect such a setup to become more and more realistic and μPMUs to become widespread for different applications [29]. Currently, different research projects are ongoing to design low-cost PMUs [30], [31] and the aim is a pervasive installation in DN [32]. In the tests, every branch is considered to be monitored by only one PMU, as in previous sections, and all the measurements are referred to the same timescale, since PMU time-tags allow alignment. The method can apply to single branches or to portions of the DN (e.g. the most important sets of branches), as discussed in Section II. Its applicability depends on the available PMUs; unobservable branches (considering also the topology constraints) cannot be included in the estimation process.

For PMU accuracy, the maximum Total Vector Error (TVE) under steady-state conditions is set equal to values typically found in the specifications of commercial PMUs. Voltage and current magnitudes and phase angle random errors have been assumed to be uniform variables (due to the lack of additional a-priori information) with maximum deviations corresponding to maximum TVE values. For example, when a maximum TVE of 0.1% is assumed in the following, maximum amplitude errors $\Delta V = 0.1\,\%$ and $\Delta I = 0.1\,\%$ are used for voltage and current synchrophasor measurements, and, maximum phase-angle errors are set to $\Delta\phi = 0.1 \cdot 10^{-2}$ rad (0.1 crad) and $\Delta\theta = 0.1$ crad. As described above, the variances and the weights are chosen according to the assumed deviations and distributions ($\sigma = \Delta/\sqrt{3}$ holds for all the considered quantities).

As discussed in previous sections, systematic errors are assumed to be associated with voltage and current transformers (VTs and CTs). For the following tests, the maximum errors for VTs and CTs are chosen according to the precision-class definitions in the standards IEC 61869 (parts 2 [23], and 3 [24]). Specifically, all transducers are considered to be of Class 0.5, and a $0.5\,\%$ maximum ratio error and 0.6 crad maximum phase displacement is used for VTs. CTs are assumed to have a maximum ratio error of $0.5\,\%$, while maximum phase displacement is 0.9 crad (that is the value indicated in [23] for current magnitudes larger than half the rated value). VT and CT maximum errors are assumed to be the maximum absolute values of the parameters ξ, α, η and ψ. The transducer errors are assumed to be uniformly distributed and thus the standard deviations are $\sqrt{3}$ times lower than the maxima.

A. Multiple cases

The first factor that plays a key role in the estimation process is the number and variety of network operating conditions included in the estimation framework. The following analysis is performed using the analytical expressions of the estimator uncertainties, given by the formulas of the variance-covariance matrix (20) of the WLS algorithm. Fig. 3 reports the standard deviation, computed from the diagonal elements of (20), of the estimated correction parameters of the line resistance and reactance (that is γ_{ij} and β_{ij}) when a single branch is considered (branch 32 of the ATLN, first branch of the third feeder) and a $-10\,\%$ deviation of line parameters is assumed (meaning $\gamma_{ij} = -0.1$ and $\beta_{ij} = -0.1$). Since correction parameters are relative values the standard deviation (std for brevity) is reported as a percentage in figures and tables for easier legibility. It is used to show the quality of the estimation

because it can be used to define the expanded uncertainty intervals around the estimated values.

Increasing the number of cases considered, which, as indicated in Section II-A, correspond to different network conditions obtained by randomly varying the loads by a maximum of $50\,\%$, allows an improved impedance estimation, but uncertainty, after a few tens of cases, cannot be significantly reduced without acting at different levels (e.g. choosing instruments with higher accuracy).

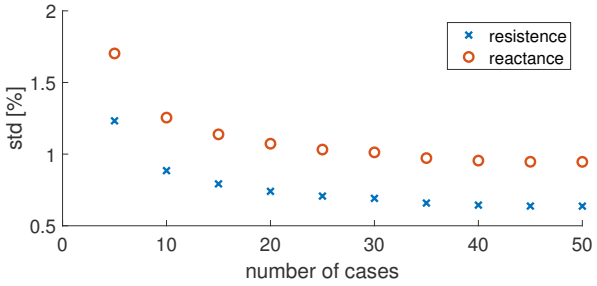

Fig. 3. Standard deviations of the estimated resistance and reactance correction parameters with a varying number of operating conditions.

Following a similar approach, results can be obtained with a fixed number of network conditions by changing the load variability level among different cases. In Fig. 4 the standard deviations of γ_{ij} and β_{ij} for the same branch are reported when 10 cases are considered, and it is clear how larger load variations lead to improved estimations. Another test, using the same number of cases, involved changing the overall network load by proportionally changing all the nominal loads in a given range (in Fig. 5 the range $60\,\% - 200\,\%$ is considered), while keeping constant the load variability level among the cases. As might be expected, heavier loading conditions lead to larger variability of node and branch power flows, allowing for operating conditions that are more distinct among cases.

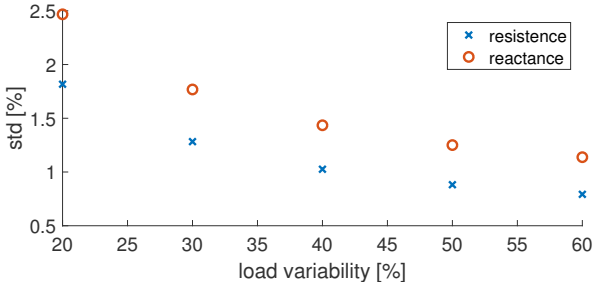

Fig. 4. Standard deviations of the estimated resistance and reactance correction parameters with a varying level of load variability.

In summary, the accuracy of the estimator strongly depends on the variety of the cases involved, since (as described in Section II-A) they add a set of constraints on the unknowns that incrementally limits their range of variability. Nevertheless, their impact on accuracy has a lower bound that depends on the accuracy of the available measurements, as can be seen in Fig. 6, where the standard uncertainty of resistance and reactance estimation for the same branch is reported with respect to the PMU accuracy in terms of TVE $\%$.

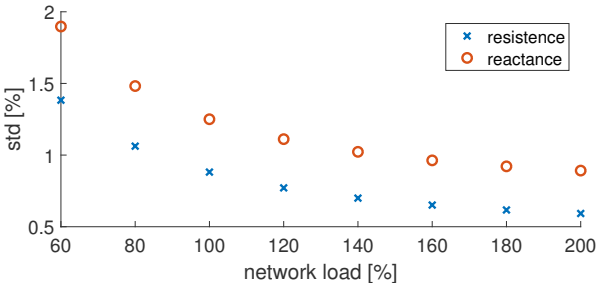

Fig. 5. Standard deviations of the estimated resistance and reactance correction parameters with a varying level of network load.

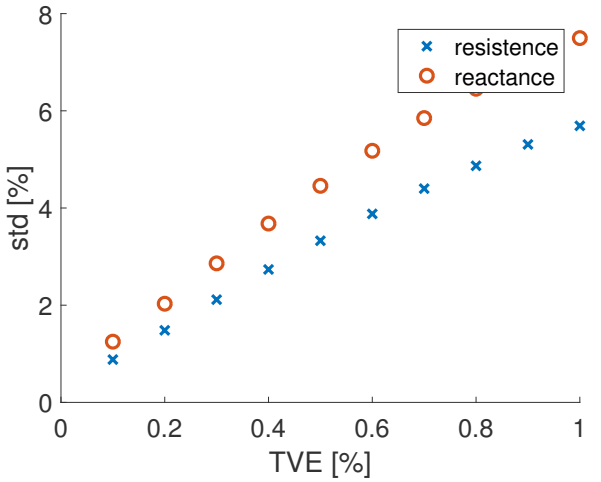

Fig. 6. Standard deviations of the estimated resistance and reactance correction parameters with a varying accuracy of PMU measurements.

B. Multiple branches

While in previous sections the achievable estimation uncertainty is investigated on a single-branch basis for analysis purposes, it is important to assess the performance of the proposed technique when the impedances of multiple branches are simultaneously estimated. With this aim, different portions of the ATLN are simultaneously estimated and the results are compared with the base case of single-branch estimation. Ten cases and ten sets of measurements for each case are used, assuming PMU accuracy is TVE $= 0.1\,\%$ and parameter variation of $-10\,\%$ as above. Table I reports the standard deviations of the estimated parameters γ (relating to line resistances) for selected branches of the network belonging to different feeders. For each reported branch, sets of 1, 2, 3 and 5 branches to which it belongs are considered, showing that the standard deviations decrease, sometimes only slightly, when a higher number of branches is considered. The influence of multiple branches on a straight line, defined as a line on which a node can be shared only between two branches, depends on the specific configuration of the branches and on the connected loads and laterals. But, it decreases when the additional branches are far from the one under consideration. The impact is mainly due to the additional constraints on each branch voltage imposed by the measurements on neighboring branches.

TABLE I
STANDARD UNCERTAINTIES OF LINE RESISTANCE CORRECTION PARAMETER FOR ESTIMATIONS INVOLVING MULTIPLE BRANCHES

Branch number	Std [%]			
	number of involved branches			
	1	2	3	5
34	2.77 %	2.74 %	2.63 %	2.61 %
70	6.46 %	6.16 %	5.54 %	5.46 %
75	5.79 %	5.41 %	5.06 %	5.06 %

Other important configurations are those corresponding to single nodes shared between multiple branches. Fig. 7 shows the percent standard deviations of the resistance and reactance estimations (two y-axes are used for the sake of clarity) when branch 1 impedance is estimated by progressively adding branches to the model. The branches added are those connected to the substation and belonging to different feeders. The uncertainty decreases with the number of branches considered and each additional constraint has a different impact on the estimation.

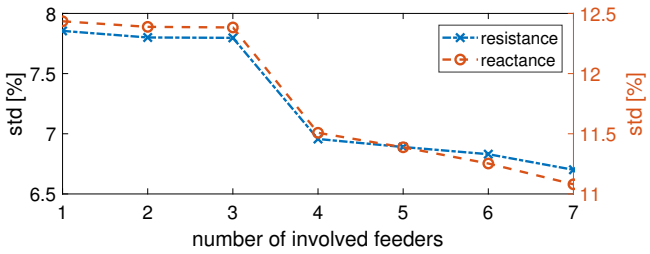

Fig. 7. Standard deviations of the estimated resistance and reactance correction parameters of branch 1 with a varying number of feeders considered.

C. Topology constraints

To investigate the role of the constraints arising when a set of nodes and branches is considered as a whole for the estimation process, a discussion of the impact of all equivalent measurements is presented. Zero injections add the equality constraints given by the KCL between the measured currents flowing in the adjacent branches. Their main impact is therefore on the accuracy of the current measurements and on the range of variability of the corresponding current transducers. Table II shows the results (same test conditions as above) in terms of standard deviations of the resistance and reactance correction parameters for two connected branches (32 and 33) when the shared node is a zero-injection node. It is clear that the additional equality constraint involving the measured currents positively affects the line impedance estimation (10 network conditions are considered as before) and the contribution is larger when a higher number of repeated measurements is considered. Repeated measurements or increased measurement accuracies clearly reduce the estimation uncertainty but also emphasize the importance of current-based constraints.

TABLE II
STANDARD UNCERTAINTIES OF LINE RESISTANCE CORRECTION PARAMETER WITH OR WITHOUT ZERO INJECTION CONSTRAINTS

Branch number	Parameter	Number of meas.	Std [%]		Variation [%]
			Without zero injection constraints	With zero injection constraints	
32	γ	10	0.99 %	0.93 %	−6.1 %
		100	0.57 %	0.46 %	−19.5 %
	β	10	1.39 %	1.29 %	−7.5 %
		100	0.86 %	0.68 %	−21.3 %
33	γ	10	1.21 %	1.16 %	−4.1 %
		100	0.60 %	0.49 %	−17.9 %
	β	10	1.67 %	1.59 %	−5.1 %
		100	0.90 %	0.73 %	−19.6 %

D. Entire Network

To complete the analysis, it is interesting to show the overall behavior on an entire network when a full set of Monte Carlo (MC) simulations is performed. This case is used to show the possibility of extending the estimation to large portions of the network, since the algorithm can work on different sets of branches depending on the available measurement system. In the following, 10 network conditions and 10 repeated measurements are used. The network parameters, transducer errors and, obviously, the measurement errors are randomly extracted from uniform distributions corresponding to their accuracy range for 1000 trials. Figures 8(a) and 8(b) show the root mean square errors (RMSE) in the estimation of the resistance and reactance, respectively, for all the network branches when line parameters can randomly vary up to 30 % with respect to nominal values. The plain line indicates the RMSEs computed on the randomly extracted impedance values (theoretically they are constant at 17.3 %), while the crosses show how the uncertainty in the estimation of the parameters varies from branch to branch, depending on the different load and topology aspects.

The corresponding average errors are much lower than the reported RMSE values (from 12 to 883 times, depending on the considered branch), thus confirming the usefulness also of the standard deviation to describe the estimation uncertainty.

Some of the branches show a small RMSE reduction with respect to the random a priori values. This occurs for short or lateral branches connected to leaves of the network tree, and, in particular, to lightly loaded branches. As an example, Fig. 9 shows the RMSE variation with load for the resistance of branch 18, which has the above characteristics (lateral and lightly loaded). Repeated tests have been performed by changing only the rated power of the attached leaf node (node 19). As expected, estimation accuracy increases with the load (1× to 5× factors are considered in Fig. 9). The estimation for such lines is tough and would require more accurate transducers and measurements. Nevertheless, it is important to highlight that such branches, precisely because of their particular characteristics, are less relevant for application level procedures relying on the line parameter knowledge, e.g. for

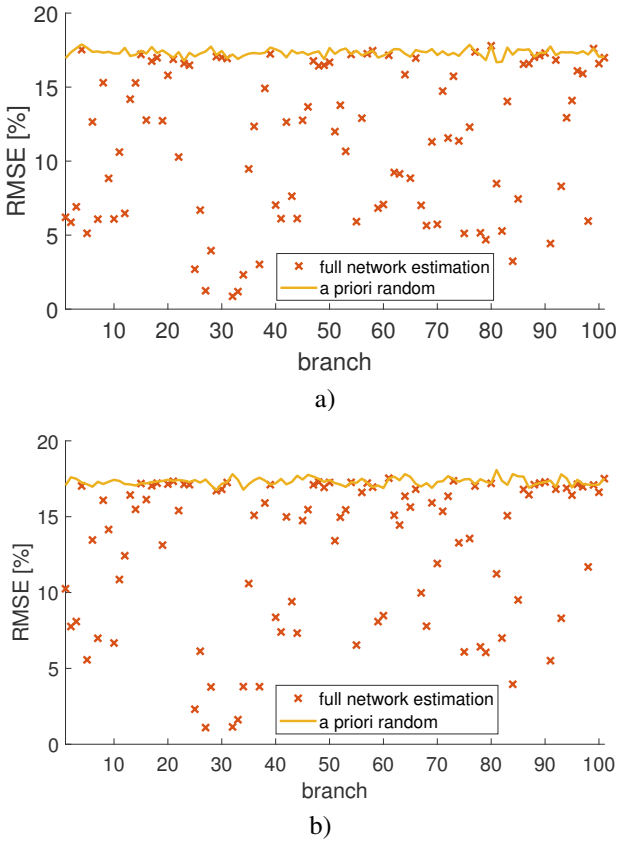

Fig. 8. Percent RMSE of the estimated line parameters: a) resistances; b) reactances.

distribution system state estimation, and thus their estimation errors are often not crucial.

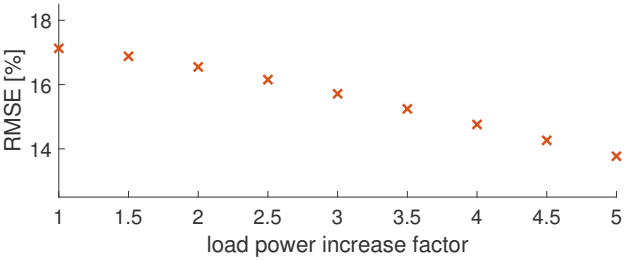

Fig. 9. Percent RMSE of the estimated line resistance of branch 18 with increasing load.

To give an idea of the impact of the proposed algorithm, it is useful to perform direct estimation of the impedance parameters by means of the measured synchronized voltage phasors at both end of each line and of the corresponding current phasor. This is the classic approach to parameter estimation and it has many issues. For a fair comparison it has been performed on exactly the same data with the same number of trials as the above test. To reduce the variability, each estimation is defined as the average of all the estimations performed with the measured synchrophasor set associated with a given timestamp. The lowest RMSE for branch resistance and reactance are, respectively, $15.66\,\%$ and $18.34\,\%$ (for branch 32 and 27, respectively), but there are many branches showing values above 100% and even far larger. This is mainly due to systematic errors that are not considered in the estimation model and can lead to extreme results, in particular for short and lightly loaded branches.

It can be observed that the proposed algorithm also allows for the estimation of transducer systematic errors (ξ, θ, η and ψ parameters), since they are included in the measurement model. Considering the above test, the amplitude ratio and phase displacement errors of the VTs can be estimated with RMSEs values up to $0.04\,\%$ and $0.04\,$crad, respectively. These values represent the remaining errors and can be compared with the VT class errors (that are, if expressed in RMS, $0.29\,\% \simeq 0.5/\sqrt{3}\,\%$ and $0.35\,\text{crad} \simeq 0.6/\sqrt{3}\,\text{crad}$, respectively). CT systematic errors can be estimated with lower accuracy, but a full investigation of the potentialities of the method for the estimation of transducers behavior is beyond the scope of this paper.

Finally, a brief discussion on computation times is reported. The average number of iterations is 4.0 (2.9 with $\delta = 10^{-5}$) and the computation time average (obtained under Matlab environment in a Windows 10 OS notebook equipped with an Intel i7 2.60 GHz CPU) on the MC trials is $6.879\,$s on the whole network and $0.002\,$s in a single-branch configuration (branch 32). The adopted accelerated algorithm that exploits repeated measurements allows a reduction of computation time in the order of $90\,\%$.

IV. Conclusion

This paper has presented an iterative algorithm to simultaneously estimate network line parameters on multiple branches using a PMU-based monitoring system. It has been shown that it takes account all transducer errors and different uncertainty sources with a sound uncertainty modelling. It was shown how multiple measurements gathered from the network under different conditions are used, thus allowing the method to simultaneously calculate network parameters on multiple branches so that relevant network topology constraints can be added and the measurement system is used to maximum effect. In future work, the proposed method can be extended to a three-phase network model using the same approach for definition of the measurement chain uncertainty.

APPENDIX A
DERIVATION OF BRANCH MEASUREMENT MODEL

From (5) and (6), using the notation of (7) and (8), it follows:

$$\begin{aligned} y_{ij}^r &\simeq h_{ij}^r(\mathbf{x}_{ij},\mathbf{e}_{ij}) = f_{ij}^r(\mathbf{x}_{ij}) + \epsilon_{ij}^r(\gamma_{ij},\beta_{ij},\mathbf{e}_{ij}) \\ &= \xi_i V_i^r - \alpha_i V_i^x - \xi_j V_j^r + \alpha_j V_j^x \\ &\quad + \eta_{ij}(X_{ij}^0 I_{ij}^x - R_{ij}^0 I_{ij}^r) + \psi_{ij}(R_{ij}^0 I_{ij}^x + X_{ij}^0 I_{ij}^r) \\ &\quad + \eta_{ij}(\beta_{ij} X_{ij}^0 I_{ij}^x - \gamma_{ij} R_{ij}^0 I_{ij}^r) \\ &\quad + \psi_{ij}(\gamma_{ij} R_{ij}^0 I_{ij}^x + \beta_{ij} X_{ij}^0 I_{ij}^r) \\ &\quad + \gamma_{ij} R_{ij}^0 I_{ij}^r - \beta_{ij} X_{ij}^0 I_{ij}^x \\ &\quad + \xi_i^{\text{PMU}} V_i^r - \alpha_i^{\text{PMU}} V_i^x - \xi_j^{\text{PMU}} V_j^r + \alpha_j^{\text{PMU}} V_j^x \\ &\quad + \eta_{ij}^{\text{PMU}}(X_{ij}^0 I_{ij}^x - R_{ij}^0 I_{ij}^r) + \psi_{ij}^{\text{PMU}}(R_{ij}^0 I_{ij}^x + X_{ij}^0 I_{ij}^r) \\ &\quad + \eta_{ij}^{\text{PMU}}(\beta_{ij} X_{ij}^0 I_{ij}^x - \gamma_{ij} R_{ij}^0 I_{ij}^r) \\ &\quad + \psi_{ij}^{\text{PMU}}(\gamma_{ij} R_{ij}^0 I_{ij}^x + \beta_{ij} X_{ij}^0 I_{ij}^r) \end{aligned} \tag{A.1}$$

$$\begin{aligned} y_{ij}^x &\simeq h_{ij}^x(\mathbf{x}_{ij},\mathbf{e}_{ij}) = f_{ij}^x(\mathbf{x}_{ij}) + \epsilon_{ij}^x(\gamma_{ij},\beta_{ij},\mathbf{e}_{ij}) \\ &= \xi_i V_i^x + \alpha_i V_i^r - \xi_j V_j^x - \alpha_j V_j^r \\ &\quad - \eta_{ij}(X_{ij}^0 I_{ij}^r + R_{ij}^0 I_{ij}^x) + \psi_{ij}(X_{ij}^0 I_{ij}^x - R_{ij}^0 I_{ij}^r) \\ &\quad - \eta_{ij}(\gamma_{ij} R_{ij}^0 I_{ij}^x + \beta_{ij} X_{ij}^0 I_{ij}^r) \\ &\quad + \psi_{ij}(\beta_{ij} X_{ij}^0 I_{ij}^x - \gamma_{ij} R_{ij}^0 I_{ij}^r) \\ &\quad + \gamma_{ij} R_{ij}^0 I_{ij}^x + \beta_{ij} X_{ij}^0 I_{ij}^r \\ &\quad + \xi_i^{\text{PMU}} V_i^x + \alpha_i^{\text{PMU}} V_i^r - \xi_j^{\text{PMU}} V_j^x - \alpha_j^{\text{PMU}} V_j^r \\ &\quad - \eta_{ij}^{\text{PMU}}(X_{ij}^0 I_{ij}^r + R_{ij}^0 I_{ij}^x) + \psi_{ij}^{\text{PMU}}(X_{ij}^0 I_{ij}^x - R_{ij}^0 I_{ij}^r) \\ &\quad - \eta_{ij}^{\text{PMU}}(\gamma_{ij} R_{ij}^0 I_{ij}^x + \beta_{ij} X_{ij}^0 I_{ij}^r) \\ &\quad + \psi_{ij}^{\text{PMU}}(\beta_{ij} X_{ij}^0 I_{ij}^x - \gamma_{ij} R_{ij}^0 I_{ij}^r) \end{aligned} \tag{A.2}$$

From (A.1) and (A.2), it is possible to see that f_{ij}^r and f_{ij}^x are analytic functions thus allowing to compute the Jacobian matrix $\mathbf{F}_{ij}$ (see full page equation (A.3)).

Considering the above expressions, the constraints are given by $\mathbf{y}_{ij} = \mathbf{f}_{ij}(\mathbf{x}_{ij}) + \epsilon(\mathbf{x}_{ij},\mathbf{e}_{ij})$. When the iterative algorithm is applied, its linearization around the temporary solution $\hat{\mathbf{x}}^q$ can be considered:

$$\begin{aligned} &\mathbf{y}_{ij} - \mathbf{f}_{ij}(\hat{\mathbf{x}}^q) \\ &= \mathbf{F}_{ij}(\hat{\mathbf{x}}^q)\Delta\hat{\mathbf{x}}_{q+1} + \epsilon(\hat{\mathbf{x}}^q,\mathbf{e}_{ij}) + \mathbf{G}_{ij}(\mathbf{e}_{ij})\Delta\hat{\mathbf{x}}_{q+1} \\ &= \mathbf{F}_{ij}(\hat{\mathbf{x}}^q)\Delta\hat{\mathbf{x}}_{q+1} + \mathbf{E}_{ij}(\hat{\mathbf{x}}^q)\mathbf{e}_{ij} + \mathbf{J}_{ij}(\mathbf{I}_n \otimes \Delta\hat{\mathbf{x}}_{q+1})\mathbf{e}_{ij} \end{aligned} \tag{A.4}$$

where $\mathbf{E}_{ij}(\mathbf{x})$ and $\mathbf{G}_{ij}(\mathbf{e}_{ij}) = \dfrac{\mathrm{d}\epsilon}{\mathrm{d}\mathbf{x}^{\mathrm{T}}}$ are detailed in (A.5) and (A.6), while n is the number of elements in $\mathbf{e}_{ij}$, $\mathbf{I}_n$ is the identity matrix and $\otimes$ indicate the Kronecker product. The last random term of (A.4) follows from $\dfrac{\mathrm{d}\mathbf{G}_{ij}(\mathbf{e}_{ij})\Delta\hat{\mathbf{x}}_{q+1}}{\mathrm{d}\mathbf{e}^{\mathrm{T}}} = \dfrac{\mathrm{d}\mathbf{G}_{ij}(\mathbf{e}_{ij})}{\mathrm{d}\mathbf{e}_{ij}^{\mathrm{T}}}(\mathbf{I}_n \otimes \Delta\hat{\mathbf{x}}_{q+1})\mathbf{e}_{ij}$ when $\mathbf{J}_{ij}$ is the constant matrix derivative of $\mathbf{G}_{ij}$ with respect to the PMU random errors (see [33]). From (A.4), considering that after a few iterations towards convergence $\Delta\hat{\mathbf{x}}_{q+1} \to \mathbf{0}$ and thus cross-multiplications of its elements with the small random errors can be neglected, the random errors can be approximated by $\mathbf{E}_{ij}(\hat{\mathbf{x}}^q)\mathbf{e}_{ij}$. From this expression the covariance matrix directly follows as $\mathbf{E}_{ij}(\hat{\mathbf{x}}^q)\mathbf{\Sigma}_{\mathbf{e}_{ij}}\mathbf{E}_{ij}(\hat{\mathbf{x}}^q)^{\mathrm{T}}$.

APPENDIX B
KCL CONSTRAINTS DERIVATION

From (12), the following relationship holds:

$$\begin{aligned} &I_j e^{j(\theta_j - \psi_j - \psi_j^{\text{PMU}})}(1 - \eta_j - \eta_j^{\text{PMU}}) \\ &\qquad = \sum_{k\in\Gamma_j} I_{jk} e^{j(\theta_{jk} - \psi_{jk} - \psi_{jk}^{\text{PMU}})}(1 - \eta_{jk} - \eta_{jk}^{\text{PMU}}) \end{aligned} \tag{B.1}$$

From (B.1), by expanding, neglecting cross-multiplications (small errors assumption), using Eulero's formula, and separating real and imaginary parts we get:

$$\begin{aligned} &I_j \cos\theta_j - \sum_{k\in\Gamma_j} I_{jk}\cos\theta_{jk} \\ &\qquad = (\eta_j + \eta_j^{\text{PMU}}) I_j \cos\theta_j - (\psi_j + \psi_j^{\text{PMU}}) I_j \sin\theta_j \\ &\qquad - I_{jk} \sum_{k\in\Gamma_j} (\eta_{jk} + \eta_{jk}^{\text{PMU}}) \cos\theta_{jk} \\ &\qquad + I_{jk} \sum_{k\in\Gamma_j} (\psi_{jk} + \psi_{jk}^{\text{PMU}}) \sin\theta_{jk} \end{aligned} \tag{B.2}$$

$$\begin{aligned} &I_j \sin\theta_j - \sum_{k\in\Gamma_j} I_{jk}\sin\theta_{jk} \\ &\qquad = (\eta_j + \eta_j^{\text{PMU}}) I_j \sin\theta_j - (\psi_j + \psi_j^{\text{PMU}}) I_j \cos\theta_j \\ &\qquad + I_{jk} \sum_{k\in\Gamma_j} (\eta_{jk} + \eta_{jk}^{\text{PMU}}) \sin\theta_{jk} \\ &\qquad + I_{jk} \sum_{k\in\Gamma_j} (\psi_{jk} + \psi_{jk}^{\text{PMU}}) \cos\theta_{jk} \end{aligned} \tag{B.3}$$

from which (13) and (14) follow. Similar passages can be applied for zero-injection constraints. From (13) and (14), the measurement functions f_j^r and f_j^x are linear with respect to the state variables and thus a constant Jacobian follows:

$$\mathbf{F}_j = \begin{bmatrix} +I_j^r & -I_j^x & \cdots & -I_{j,k}^r & +I_{j,k}^x & \cdots \\ +I_j^x & +I_j^r & \cdots & -I_{j,k}^x & -I_{j,k}^r & \cdots \end{bmatrix} \tag{B.4}$$

and, considering (13) and (14) with zero injection current and no additional unknowns, the zero-injection equivalent measurement functions are linear and lead to the following constant Jacobian:

$$\mathbf{F}_{j-zero} = \begin{bmatrix} \cdots & -I_{j,k}^r & +I_{j,k}^x & \cdots \\ \cdots & -I_{j,k}^x & -I_{j,k}^r & \cdots \end{bmatrix} \tag{B.5}$$

Since no network parameters are involved in the KCL the above Jacobians are constant and do not depend on the algorithm iteration index.

The covariance matrix of these couples of equivalent measurements is obtained by a first order uncertainty propagation law as:

$$\mathbf{\Sigma}_{\epsilon_j} = \mathbf{E}_j \mathbf{\Sigma}_{\mathbf{e}_j} \mathbf{E}_j^{\mathrm{T}} \tag{B.6}$$

and

$$\mathbf{\Sigma}_{\boldsymbol{\epsilon}_{j-zero}} = \mathbf{E}_{j-zero} \mathbf{\Sigma}_{\mathbf{e}_{j-zero}} \mathbf{E}_{j-zero}^{\mathrm{T}} \tag{B.7}$$

where $\mathbf{e}_j$ is the vector including η_j^{PMU}, ψ_j^{PMU} and all the involved η_{jk}^{PMU} and ψ_{jk}^{PMU} of adjacent branch measurements, while $\mathbf{e}_{j-zero}$ is the vector of the involved η_{jk}^{PMU} and ψ_{jk}^{PMU}. $\mathbf{\Sigma}_{\mathbf{e}_j}$ and $\mathbf{\Sigma}_{\mathbf{e}_{j-zero}}$ are diagonal matrices and their elements are the variances of all the η_{jk}^{PMU} and ψ_{jk}^{PMU}.

$$\mathbf{F}_{ij} = \left[\begin{array}{cccc} V_i^r & -V_i^x & -V_j^r & V_j^x \\ V_i^x & V_i^r & -V_j^x & -V_j^r \end{array} \right.$$
$$\begin{array}{cc} -(1+\gamma_{ij})R_{ij}^0 I_{ij}^r + (1+\beta_{ij})X_{ij}^0 I_{ij}^x & (1+\gamma_{ij})R_{ij}^0 I_{ij}^x + (1+\beta_{ij})X_{ij}^0 I_{ij}^r \\ -(1+\gamma_{ij})R_{ij}^0 I_{ij}^x - (1+\beta_{ij})X_{ij}^0 I_{ij}^r & -(1+\gamma_{ij})R_{ij}^0 I_{ij}^r + (1+\beta_{ij})X_{ij}^0 I_{ij}^x \\ (1-\eta_{ij})R_{ij}^0 I_{ij}^r + \psi_{ij} R_{ij}^0 I_{ij}^x & -(1-\eta_{ij})X_{ij}^0 I_{ij}^x + \psi_{ij} X_{ij}^0 I_{ij}^r \\ (1-\eta_{ij})R_{ij}^0 I_{ij}^x - \psi_{ij} R_{ij}^0 I_{ij}^r & +(1-\eta_{ij})X_{ij}^0 I_{ij}^r + \psi_{ij} X_{ij}^0 I_{ij}^x \end{array} \left. \right] \quad \text{(A.3)}$$

$$\mathbf{E}_{ij} = \left[\begin{array}{cccc} V_i^r & -V_i^x & -V_j^r & V_j^x \\ V_i^x & V_i^r & -V_j^x & -V_j^r \end{array} \right.$$
$$\left. \begin{array}{cc} -(1+\gamma_{ij})R_{ij}^0 I_{ij}^r + (1+\beta_{ij})X_{ij}^0 I_{ij}^x & (1+\gamma_{ij})R_{ij}^0 I_{ij}^x + (1+\beta_{ij})X_{ij}^0 I_{ij}^r \\ -(1+\gamma_{ij})R_{ij}^0 I_{ij}^x - (1+\beta_{ij})X_{ij}^0 I_{ij}^r & -(1+\gamma_{ij})R_{ij}^0 I_{ij}^r + (1+\beta_{ij})X_{ij}^0 I_{ij}^x \end{array} \right] \quad \text{(A.5)}$$

$$\mathbf{G}_{ij} = \left[\begin{array}{cccccc} 0 & 0 & 0 & 0 & 0 & 0 \\ 0 & 0 & 0 & 0 & 0 & 0 \end{array} \right.$$
$$\left. \begin{array}{cc} -\eta_{ij}^{\text{PMU}} R_{ij}^0 I_{ij}^r + \psi_{ij}^{\text{PMU}} R_{ij}^0 I_{ij}^x & \eta_{ij}^{\text{PMU}} X_{ij}^0 I_{ij}^x + \psi_{ij}^{\text{PMU}} X_{ij}^0 I_{ij}^r \\ -\eta_{ij}^{\text{PMU}} R_{ij}^0 I_{ij}^x - \psi_{ij}^{\text{PMU}} R_{ij}^0 I_{ij}^r & -\eta_{ij}^{\text{PMU}} X_{ij}^0 I_{ij}^r + \psi_{ij}^{\text{PMU}} X_{ij}^0 I_{ij}^x \end{array} \right] \quad \text{(A.6)}$$

APPENDIX C
ATLANTIDE NETWORK

Table III reports the resistance and reactance parameters per unit length of the 102-node ATLANTIDE Italian rural network used for the tests. For space reasons, only the first 5 branches (Feeder 1) are reported as a sample of the values.

TABLE III
LINE PARAMETERS OF THE ATLANTIDE NETWORK (FEEDER 1)

Branch number	**Resistance** [Ω/km]	**Reactance** [Ω/km]	**length** [km]
1	0.254	0.126	1.37
2	0.166	0.110	3.07
3	0.517	0.387	0.80
4	0.466	0.349	0.90
5	0.689	0.515	1.33
...	...	...	...

ACKNOWLEDGEMENTS

The work of P. A. Pegoraro, P. Castello and C. Muscas has been partially funded by Fondazione di Sardegna for the research project "ODIS - Optimization of DIstributed systems in the Smart-city and smart-grid settings" - Convenzione triennale tra la Fondazione di Sardegna e gli Atenei Sardi Regione Sardegna – L.R. 7/2007 annualità 2016 – DGR 28/21 del 17.05.2015.

REFERENCES

[1] *IEEE Standard for Synchrophasor Measurements for Power Systems*, IEEE IEEE Std C37.118.1-2011 (Revision of IEEE Std C37.118-2005), Dec. 2011.

[2] A. von Meier, D. Culler, A. McEachern, and R. Arghandeh, "Micro-synchrophasors for distribution systems," in *ISGT 2014*, Feb 2014, pp. 1–5.

[3] P. Castello, P. Ferrari, A. Flammini, C. Muscas, and S. Rinaldi, "A new IED with PMU functionalities for electrical substations," *IEEE Transactions on Instrumentation and Measurement*, vol. 62, no. 12, pp. 3209–3217, 2013.

[4] P. A. Pegoraro, A. Meloni, L. Atzori, P. Castello, and S. Sulis, "Pmu-based distribution system state estimation with adaptive accuracy exploiting local decision metrics and iot paradigm," *IEEE Transactions on Instrumentation and Measurement*, vol. 66, no. 4, pp. 704–714, Apr. 2017.

[5] *IEEE Standard for Synchrophasor Data Transfer for Power Systems*, IEEE IEEE Std C37.118.2-2011 (Revision of IEEE Std C37.118-2005), Dec. 2011.

[6] AA. VV., *Phasor Measurement Units and Wide Area Monitoring Systems*, 1st ed. Academic Press, 2016.

[7] S. Chakrabarti and E. Kyriakides, "Pmu measurement uncertainty considerations in wls state estimation," *IEEE Transactions on Power Systems*, vol. 24, no. 2, pp. 1062–1071, May 2009.

[8] F. Aminifar, M. Shahidehpour, M. Fotuhi-Firuzabad, and S. Kamalinia, "Power system dynamic state estimation with synchronized phasor measurements," *IEEE Transactions on Instrumentation and Measurement*, vol. 63, no. 2, pp. 352–363, 2014.

[9] G. N. Korres, N. M. Manousakis, T. C. Xygkis, and J. Löfberg, "Optimal phasor measurement unit placement for numerical observability in the presence of conventional measurements using semi-definite programming," *IET Generation, Transmission Distribution*, vol. 9, no. 15, pp. 2427–2436, 2015.

[10] D. Ritzmann, J. Rens, P. S. Wright, W. Holderbaum, and B. Potter, "A novel approach to noninvasive measurement of overhead line impedance parameters," *IEEE Transactions on Instrumentation and Measurement*, vol. 66, no. 6, pp. 1155–1163, 2017.

[11] P. Zarco and A. G. Exposito, "Power system parameter estimation: a survey," *IEEE Transactions on power systems*, vol. 15, no. 1, pp. 216–222, 2000.

[12] G. Kusic and D. Garrison, "Measurement of transmission line parameters from scada data," in *Power Systems Conference and Exposition, 2004. IEEE PES*, Oct 2004, pp. 440–445 vol.1.

[13] D. Ritzmann, P. S. Wright, W. Holderbaum, and B. Potter, "A method for accurate transmission line impedance parameter estimation," *IEEE Transactions on Instrumentation and Measurement*, vol. 65, no. 10, pp. 2204–2213, 2016.

[14] R. E. Wilson, G. A. Zevenbergen, D. L. Mah, and A. J. Murphy, "Calculation of transmission line parameters from synchronized measurements," *Electric Machines &Power Systems*, vol. 27, no. 12, pp. 1269–1278, 1999.

[15] D. Shi, D. J. Tylavsky, N. Logic, and K. M. Koellner, "Identification of short transmission-line parameters from synchrophasor measurements," in *Power Symposium, 2008. NAPS'08. 40th North American*, 2008, pp. 1–8.

[16] Y. Liao and M. Kezunovic, "Online optimal transmission line parameter estimation for relaying applications," *IEEE Trans. Power Del.*, vol. 24, no. 1, pp. 96–102, 2009.

[17] C. Mishra, V. A. Centeno, and A. Pal, "Kalman-filter based recursive regression for three-phase line parameter estimation using synchrophasor measurements," in *Power & Energy Society General Meeting, 2015 IEEE*, 2015, pp. 1–5.

[18] M. Asprou and E. Kyriakides, "Identification and estimation of erroneous transmission line parameters using pmu measurements," *IEEE Trans. Power Del.*, 2017.

[19] A. M. Prostejovsky, O. Gehrke, A. M. Kosek, T. Strasser, and H. W. Bindner, "Distribution line parameter estimation under consideration of measurement tolerances," *IEEE Transactions on Industrial Informatics*, vol. 12, no. 2, pp. 726–735, Apr. 2016.

[20] B. Das, "Estimation of parameters of a three-phase distribution feeder," *IEEE Trans. Power Del.*, vol. 26, no. 4, pp. 2267–2276, Oct. 2011.

[21] P. A. Pegoraro, P. Castello, C. Muscas, K. Brady, and A. von Meier, "Handling instrument transformers and PMU errors for the estimation of line parameters in distribution grids," in *2017 IEEE International Workshop on Applied Measurements for Power Systems (AMPS)*, Sept 2017, pp. 1–6.

[22] M. Pau, P. A. Pegoraro, and S. Sulis, "Efficient branch-current-based distribution system state estimation including synchronized measurements," *IEEE Transactions on Instrumentation and Measurement*, vol. 62, no. 9, pp. 2419–2429, Sep. 2013.

[23] *IEC 61869-2:2012-11: Instrument transformers - Part 2: Additional requirements for current transformers*, IEC IEC, 2012.

[24] *IEC 61869-3:2011-10: Instrument transformers Part 3: Additional requirements for inductive voltage transformers*, IEC Std., 2011.

[25] M. Asprou, E. Kyriakides, and M. Albu, "The effect of pmu measurement chain quality on line parameter calculation," in *Instrumentation and Measurement Technology Conference (I2MTC), 2017 IEEE International*, 2017, pp. 1–6.

[26] Y. Sun, T. Williams, and S. N. Gourisetti, "A comparative study of distribution system parameter estimation methods," in *2016 IEEE Power and Energy Society General Meeting (PESGM)*, July 2016, pp. 1–5.

[27] U. Kuhar, M. Pantos, G. Kosec, and A. Svigelj, "The impact of model and measurement uncertainties on a state estimation in three-phase distribution networks," *IEEE Transactions on Smart Grid*, pp. 1–1, Apr 2018.

[28] A. Bracale, R. Caldon, G. Celli, M. Coppo, D. D. Canto, R. Langella, G. Petretto, F. Pilo, G. Pisano, D. Proto, S. Scalari, and R. Turri, "Analysis of the italian distribution system evolution through reference networks," in *2012 3rd IEEE PES Innovative Smart Grid Technologies Europe (ISGT Europe)*, Oct 2012, pp. 1–8.

[29] A. von Meier, E. Stewart, A. McEachern, M. Andersen, and L. Mehrmanesh, "Precision micro-synchrophasors for distribution systems: A summary of applications," *IEEE Transactions on Smart Grid*, vol. 8, no. 6, pp. 2926–2936, Nov. 2017.

[30] A. Angioni, G. Lipari, M. Pau, F. Ponci, and A. Monti, "A low cost pmu to monitor distribution grids," in *2017 IEEE International Workshop on Applied Measurements for Power Systems (AMPS)*, Sep. 2017, pp. 1–6.

[31] P. Tosato, D. Macii, M. Luiso, D. Brunelli, D. Gallo, and C. Landi, "A tuned lightweight estimation algorithm for low-cost phasor measurement units," *IEEE Transactions on Instrumentation and Measurement*, vol. 67, no. 5, pp. 1047–1057, May 2018.

[32] M. Pignati, M. Popovic, S. Barreto, R. Cherkaoui, G. D. Flores, J. Y. L. Boudec, M. Mohiuddin, M. Paolone, P. Romano, S. Sarri, T. Tesfay, D. C. Tomozei, and L. Zanni, "Real-time state estimation of the epfl-campus medium-voltage grid by using pmus," in *2015 IEEE Power Energy Society Innovative Smart Grid Technologies Conference (ISGT)*, Feb. 2015, pp. 1–5.

[33] G. D'Antona, "Measurement data processing using random matrices: a generalized formula for the propagation of uncertainty," *IEEE Trans. Instrum. Meas.*, vol. 53, no. 2, pp. 537–545, April 2004.

Paolo Attilio Pegoraro (M'06) received the M.S. (summa cum laude) degree in telecommunications engineering and the Ph.D. degree in electronic and telecommunications engineering from the University of Padova, Padua, Italy, in 2001 and 2005, respectively.

He is currently an Assistant Professor of electrical and electronic measurements with the Department of Electrical and Electronic Engineering, University of Cagliari, Cagliari, Italy. He received the National Scientific Qualification to function as an Associate Professor in 2017.

He has authored or co-authored over 80 scientific papers. His current research interests include the development of new architectures and measurement techniques for the monitoring of modern power networks, with particular attention to synchronized measurements and state estimation for distribution grids.

Dr. Pegoraro is a member of the IEEE Instrumentation and Measurement Society TC-39 - Measurements in Power Systems.

Kyle Brady is a PhD candidate in electrical engineering at the University of California, Berkeley. His research has focused on distribution synchrophasors, controls, and optimal power flow. Before beginning his graduate degree, Kyle received his B.A. in physics from U.C. Berkeley and spent three years as a research assistant for the RAND Corporation.

Paolo Castello (S'11–M'15) received the M.S. degree in Electronic Engineering and the Ph.D. degree in Electronic and Computer Engineering from the University of Cagliari in 2010 and in 2014, respectively. Currently, he is assistant professor in the Electrical and Electronic Measurements Group of the Department of Electrical and Electronic Engineering at the University of Cagliari. His research activity focuses on the development of algorithms for synchrophasor calculation, the characterization and testing of Phasor Measurement Units, and design of new monitoring architectures for power systems based on IEC 61850 standard.

Carlo Muscas (M'98, SM'15) received the M.S. (cum laude) degree in electrical engineering from the University of Cagliari, Cagliari, Italy, in 1994.

He was Assistant Professor (from 1996 to 2001) and Associate Professor (from 2001 to 2017) with the University of Cagliari. Since 2017 he has been a Full Professor of Electrical and Electronic Measurement with the University of Cagliari, where he is currently the Chairman of the Council for the B. S. degree in Electrical, Electronic and Computer Engineering.

His current research interests include the measurement of synchronized phasors, the implementation of distributed measurement systems for modern electric grid, and the study of power quality phenomena.

He has authored and co-authored more than 130 scientific papers and is currently the Chairman of TC 39 (Measurements in Power Systems) of IEEE Instrumentation and Measurement Society.

Alexandra von Meier (M'10) is an Adjunct Professor of Electrical Engineering and Computer Science at the University of California, Berkeley, and Director of Electric Grid Research at the California Institute for Energy and Environment. She was previously a Professor of Energy Management and Design at Sonoma State University. She received her PhD in Energy and Resources at UC Berkeley in 1995.